Monitoring long-term evolution of engineered barrier systems using magnets

Journal of Hazardous Materials 341 (2018) 28–35

Contents lists available at ScienceDirect

Journal of Hazardous Materials

journal homepage: www.elsevier.com/locate/jhazmat

Research Paper

Monitoring long-term evolution of engineered barrier systems using magnets: Magnetic response

N. Rigonat[a,*], O. Isnard[b,c], S.L. Harley[a], I.B. Butler[a]

[a] School of Geosciences, The University of Edinburgh, James Hutton Road, EH9 3FE, United Kingdom
[b] CNRS, Institut NéEL, 25 rue des Martyrs, BP166, F-38042 Grenoble Cédex 9, France
[c] Université Grenoble Alpes, Inst. NéEL, BP166, F-38042 Grenoble, France

HIGHLIGHTS

- Nd-Fe-B magnets show time-dependent transition from ferromagnetic square-like to superparamagnetic loops upon corrosion.
- The changes in the hysteretic and thermomagnetic behaviour of Nd-Fe-B are related to the formation of hydride phases.
- SmCo magnets feature changes of the coercive field but not of the intrinsic hysteretic properties due to hydrides formation.
- AlNiCo magnets feature negligible deviations in remanence and saturation magnetization.

ARTICLE INFO

Article history:
Received 8 November 2016
Received in revised form 28 May 2017
Accepted 27 June 2017
Available online 28 June 2017

Keywords:
Engineered barrier systems
Nd-Fe-B
SmCo
AlNiCo
Bentonite

ABSTRACT

Remote and non-destructive monitoring of the stability and performance of Engineered Barrier Systems for Geological Disposal Facility of is gaining considerable importance in establishing the safety cases for Higher Activity Wastes disposal. This study offers an innovative use of mineral magnetism for monitoring groundwater saturation of the barrier. Four mixtures of permanent magnets (Nd-Fe-B, coated and uncoated; SmCo and AlNiCo) and bentonite were reacted for 4, 8 and 12 months with mildly-saline, high-pH leachates, representing the fluids saturating a time-evolved engineered barrier. Coupled hysteresis and thermomagnetic analyses demonstrate how Nd-Fe-B feature a time-dependent transition from square-like ferromagnetic to superparamagnetic loop via pot-bellied and wasp-waist loops, whereas SmCo and AlNiCo do not show so extensive corrosion-related variations of the intrinsic and extrinsic magnetic properties. This study allowed to identify magnetic materials suitable for shorter- (Nd-Fe-B) and longer-term (SmCo and AlNiCo) monitoring purposes.

1. Introduction

One of the essential features of Geological Disposal Facility (GDF) concepts for the disposal of high-level radioactive waste in the deep sub-surface is the protection of radioactive waste canisters from corrosion in order to avoid or at least minimise the release of radionuclides into the near-field environment and beyond. To achieve this most Waste Management Organisations (WMOs) have developed safety cases based on the cumulative properties of multi-barrier systems composed by the waste canister, a bentonite sleeve around the canister with a thickness around 1 m and finally the geosphere itself.

The performance of the clay-based backfill material is a crucial factor to establish the safety case for the deep underground nuclear waste disposal; the backfill material should maintain its peculiar physico-chemical-mechanical characteristics, like very low porosity and hydraulic conductivity, through time.

However, the bentonite buffer will undergo mineralogical transformations that will affect its physio-chemical-mechanical properties because of interaction with hyperalkaline leachates coming from cementiferous backfill, Fe enrichment in the vicinities of the canister or ingress of groundwaters rich in potassium.

Monitoring of the GDF and its constituent parts is recognised internationally as being critical to decision-making during phased or staged disposal of radioactive waste [1,2]. Monitoring, via continuous or periodic observation and measurement, of the key thermal, mechanical, chemical and hydrological parameters of a GDF is not only required in order to evaluate the behaviour of the repository system and performance of the barriers in relation to their

* Corresponding author.
E-mail addresses: Nicola.Rigonat@ed.ac.uk, Nicola.Rigonat@icloud.com (N. Rigonat).

http://dx.doi.org/10.1016/j.jhazmat.2017.06.064

safety functions, but also to build and sustain public confidence in geological disposal [1–4].

Whilst the need for pre-construction and operational monitoring of a GDF is fully accepted by all WMOs and national programmes in accord with the requirements of the IAEA [3,5], the need for post-closure monitoring has until recently been questioned. One reason for this is that closure of a GDF would only occur once it is deemed, on the basis of all the pre- and operational monitoring coupled with forward modelling, to meet the standards required for post-closure safety.

As discussed in a previously published paper by Harley et al. most of the tested monitoring techniques require a power source to operate and their ability to monitor the useful parameters for the Engineered Barrier System (EBS) evolution is limited.

Hence, Harley et al. developed an alternative approach to in-situ monitoring of any bentonite-based EBS using magnetic materials; the concept underpinned in that study was on utilizing fluid-induced changes in the intrinsic magnetic properties of natural and synthetic materials to monitor the migration and recharge of fluids into the EBS of a bentonite-buffered GDF for high level waste.

This work represents a further refinement of the experiment described by Harley et al. [6], with the magnets/bentonite samples reacted in an environment considered being closer to the conditions of a time-evolved EBS. This paper investigates the effects of the corrosion process on the magnetic properties of the embedded magnets only; the evolution of the bentonite matrix will be investigated in another publication.

2. Literature review

Over the past few decades research on the development of new permanent magnets has been promoted by the singular importance of these materials for a vast range of industrial and civil applications, ranging from informatics to medical technologies and space industry; these synthetic magnets are gaining even more importance with the increasing quest to increase renewable energy in global electricity production.

2.1. Nd-Fe-B permanent magnets

Research on corrosion studies of Nd-Fe-B permanent magnets has increased in importance in the light of increasing demand of electric engines for fuel-free cars, turbines for windfarms and green energy power plants. Corrosion kinetics and their dependence on temperature and environmental conditions (especially in humid environments) have been extensively studied [7–11]. However, less work has been done on the corrosion in wet environments and in saturated and unsaturated soils.

The tetragonal Nd-Fe-B alloy structure has a high uniaxial magnetocrystalline anisotropy, which gives the compound a high resistance to demagnetization and a very high saturation magnetization. In an Nd-Fe-B alloy three phases can be defined: the matrix is made of a ferromagnetic tetragonal $Nd_2Fe_{14}B$ phase (φ-phase) and is surrounded by intergranular regions containing a neodymium-rich phase (ρ-phase) $Nd_5Fe_2B_6$ [12–15] and a B-rich phase (η) $Nd_{1+x}Fe_4B_4$ [16,17]

Several studies relate the corrosion properties of these alloys with the magnets microstructure [7–9,18], and others point out the important role played by hydrogen [16,19–21]. The corrosion of Nd-Fe-B magnets can cause a worsening of their magnetic properties, loss of mechanical properties, and sometimes disaggregation of the magnets to fine powders. These effects are mainly related to the presence of the multiple phases within the magnet and their completely different electrochemical properties.

Sugimoto et al. [22] studied the corrosion rates of the three phases in a neutral borate-boric acid buffered solution and found that these increase from the φ-phase to the η-phase. This means that the η- and subsequentely the ρ-phase dissolve preferentially, resulting in localized intergranular corrosion, which continues until the φ-phase grains break apart, creating a disaggregated powder [18]. The ρ-phase on the surface of the magnets reacts with water vapour and oxygen in a hot, humid atmosphere with hydrogen generated from the decomposition of water vapour reacting with the Nd [17]. The volume expansion of the ρ-phase along the grain boundaries results in the dislodgement or exfoliation of the grains of the φ-phase, which form separate powderized granules [18]. One of the main causes of loss of coercive field in Nd-Fe-B magnets is regarded to be hydrogen absorption by the φ-phase [19], and the hydrogen decrepitation and corrosion which takes place in the Nd-Fe-B alloys has been attributed to the formation of hydrides [23]. Only few papers have investigated the correlation between the hydrogenation process and corrosion [16,21].

2.2. SmCo permanent magnets

Sintered Samarium Cobalt magnets (SmCo) were the first of the Rare Earth permanent magnet family. RE_2TM_{17} (Rare-Earth Element and Transition Metal) type magnets originated from the investigation of $R_2(Co, Fe)_{17}$ alloys in 1972 [24]. Commercial SmCo magnets have a standard formula $Sm_2(Co, Fe, Cu, Zr)_{17}$ but they are divided into two grades [25].

The microstructure of the Sm_2Co_{17} alloys has been extensively characterised by several authors [26–28]. It consists of Sm_2Co_{17} cells of the order of 100 nm in size surrounded by boundaries of $SmCo_5$, and penetrated by thin Zr-rich lamellae perpendicular to the c-axis. On a larger scale, this structure is divided into equigranular grains approximately 40–50 μm across and interspersed with 2–5 μm particles of Sm oxide formed during alloy production [29].

Pragnell et al. [29] heated two grades af SmCo magnets (one standard grade and one "high temperature" grade) at temperatures between 300 and 600 °C, for up to 1000 h at the lower temperatures and up to 350 h for the highest temperatures. Both SmCo grades exhibited two main oxidation processes. A thin oxide scale formed on the exterior surface of the alloy and an internal reaction zone was found to grow into the substrate; the external oxide layer was highly adherent with no tendency to spall and a thickness of no more than 10–15 μm after 300 h at 600 °C. Based on the EDX element mapping in conjunction with XRD measurements the outermost oxide was found to be CuO, with a thin layer of Co_3O_4 just below it. The thickest corrosion-produced layer, just above the underlying alloy, was $CoFe_2O_4$. The oxides appeared to be layered in order of their thermodynamic stability (i.e. $CuO/Co_3O_4/CoFe_2O_4$)[29].

2.3. AlNiCo permanent magnets

Alnico magnets were developed in the 1930′s and were the first "Real" performance permanent magnets. McCaig [30] used the term Al-Ni-Co to describe all permanent magnets based on the Al-Ni-Fe system. The commercial grade AlNiCo magnets have these main elements percentages by weight: Aluminium 6–13%, Nickel 13–26%, Cobalt 0–42%, Copper 2–6%, Titanium 0–9%, Niobium 0–3% and balancing Iron (30–40%). Their magnetic anisotropy and consequently coercive field are due to shape anisotropy arising from a dedicated columnar microstructure favoured by the metallurgical process. AlNiCo permanent magnets are considered being very stable and usually do not require protective coating, unless exposed to salt water or strong alkali solutions because they contain some free elemental iron and so may be prone to surface corrosion.

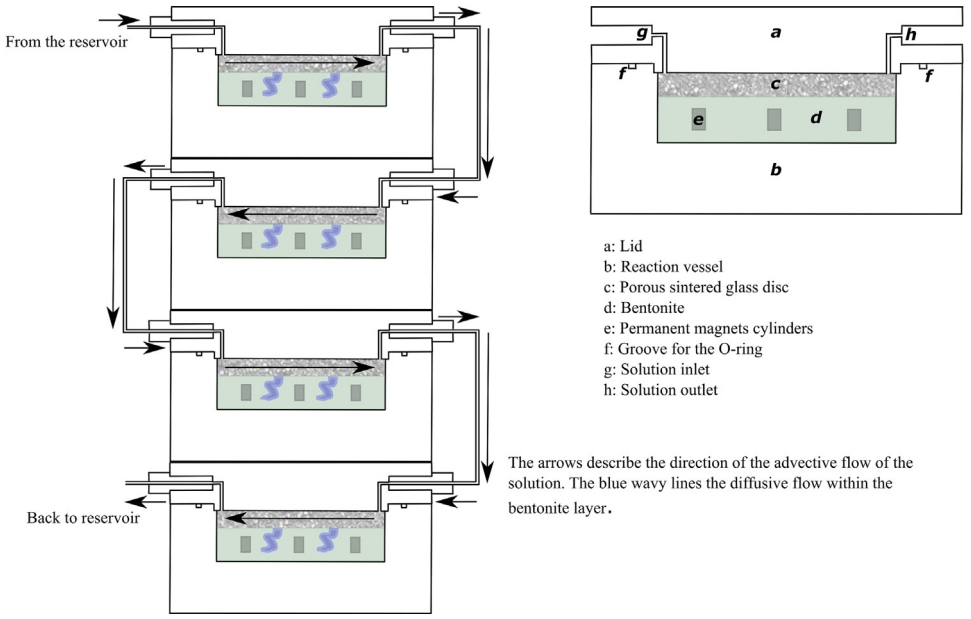

Fig. 1. Diagram of the experimental set-up.

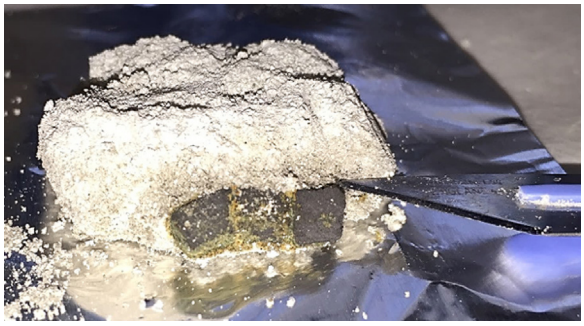

Fig. 2. Post-extraction picture of the corroded uncoated NdFeB magnets still encased in the bentonite matrix. Tip of the scalpel used as a reference.

3. Materials and methods

This experiment was designed to deliver chemical boundary conditions similar to those expected in a time-evolved GDF. Different mixtures of powderized MX80 bentonite (a clay belonging to the smectite group) and permanent magnets were reacted with a high-pH mildly saline solution (0.27 M NaCl solution reacted with Nirex Reference Vault Backfill (NRVB) cement [31] to produce a leachate with pH between 12 and 12.5) for different times at 70 °C. The solution reservoirs were purged with nitrogen gas to guarantee leaching of the cement in dysoxic conditions and the resultant solution was circulated through the reaction stacks with a multi-head peristaltic pump with a flow rate of 3 mL/min.

In the experiments three kind of permanent magnets were used

- Grade N42 Nd-Fe-B permanent magnets (Ni-Cu-Ni coated and non-coated).
- Grade SmCo26 (Sm_2Co_{17}-type) non-coated.
- Grade 5 AlNiCo permanent magnets, non-coated.

The reaction cells (Fig. 1) were based on a design similar to the transport cells developed by Fernandez et al., [32] and reaction cells developed by Fernandez et al., [33]. In a stack, each cell of the four was connected to the following by a fluid advection system. The bentonite/magnet mixture was sitting in a reaction vessel made of Delrin® homopolymer and covered with a porous sinter glass disc and exposed on its upper surface to the alkaline solution and was allowed to interact with the solution by diffusive processes only. The reaction vessels were stacked one above each other in order to allow the solution to circulate from the top to the bottom vessel and then to be recycled in the water reservoir (Fig. 1).

Three stacks of four vessels (containing coated Nd-Fe-B, uncoated Nd-Fe-B, SmCo and AlNiCo magnets respectively) were prepared for extraction after different periods (4, 8 and 12 months). One of the SmCo experiments was aborted after 5 months due to a failure of the sealing system of the cell.

The materials (raw and reacted) were characterised for Curie Points and magnetization analysis. For the thermomagnetic measurements, a home-made Faraday type balance was used; the magnetic field used was less than 0.1 T. The thermomagnetic measurements were performed with a heating rate of 10 °C/min on powder samples the measurements have been carried out from room temperature up to 900 °C (Nd-Fe-B) and 1000 °C (SmCo and AlNiCo). A sample of 50–100 mg was sealed under vacuum in a small silica tube in order to prevent oxidation of the sample during heating.

The magnetization measurements of the SmCo type magnets have been performed in magnetic field up to 10T using the extraction method in an homemade experimental set up that has been described elsewhere [34]. The saturation magnetization M_S was determined through extrapolation from the M vs. 1/H plot, with the law of approach to saturation used for the fit of the curve.

A similar equipment running in temperature ranges from 200 to 850 K and magnetic field up to 7T has been used for other series of compounds exhibiting less magnetic anisotropy and coercitivities.

Nd-Fe-B magnets were also characterised using Powder X-ray Diffraction; the samples were mixed with pure reagent grade germanium [16] and then scanned with the following parameters 22–85°2θ, 0.01 step size and 4 s step time using a Bruker D8 advance with Sol-X Energy dispersive detector. Semi quantitative analysis were performed using Bruker DIFFRAC·EVA software using structural files downloaded from the CDS-RCS (national Chemical Database Service – Royal Society of Chemistry) online database.

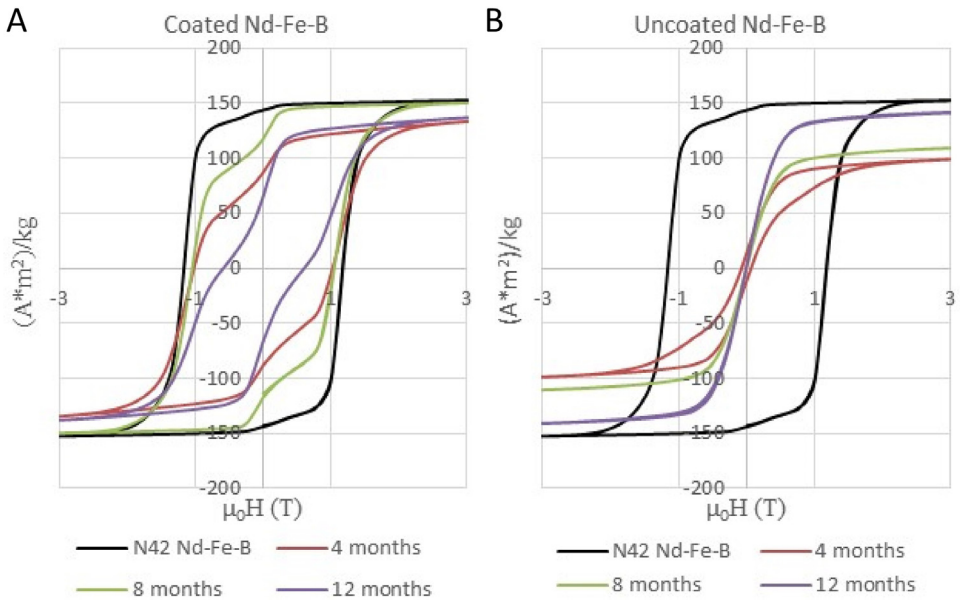

Fig. 3. Hysteresis loops of coated Nd-Fe-B samples (A) and uncoated Nd-Fe-B samples (B).

Table 1
List of hysteretic properties and Curie temperatures of the Nd-Fe-B samples. Two of the samples of the uncoated Nd-Fe-B failed the thermomagnetic analysis. One (12 months) exploded during the experiment and the other (4 months) showed complete loss of thermomagnetic properties above RT.

	Duration (months)	Weight (gr)	Coercive field (T)	Remanent specific magn. (A^*m^2)/kg	Specific saturation magn. (A^*m^2)/kg	T_C (°C)
Raw		0.3172	1.2	145.3	152.83	310
Coated	4	0.3190	1.1	84	131.03	310 (330)
	8	0.3189	1.1	117.5	149.57	310 (330)
	12	0.3189	0.61	65.8	135.46	350
Uncoated	4	0.2196	0.1	12.9	87.9	not measured
	8	0.2465	0	0	96.95	380
	12	0.2356	0	0	121.39	not measured

Table 2
results of the semi-quantitative analysis on the composition of the main magnetic phase. Values expressed in percentage and normalised to 100%.

	Duration (months)	$Nd_2Fe_{14}B$	$Nd_2Fe_{14}BH_2$	$Nd_2Fe_{14}BH_3$	$Nd_2Fe_{14}BH_5$
Raw		100	0	0	0
Coated	4	84	0	8	8
	8	89	7	3	1
	12	79	9	8	4
Uncoated	4	30	5	62	3
	8	42	8	46	4
	12	19	71	0	10

4. Experimental results

At the time of the extraction, the four kind of magnets showed different corrosion characteristics: the uncoated Nd-Fe-B magnets were extremely fragile and coated by black-coloured precipitates (Fig. 2) and disaggregated steadily during separation from the clay matrix, whereas the other magnets were all intact and showed presence of dark-grey or orange-coloured precipitates.

4.1. Nd-Fe-B magnets

The results of the magnetization measurements on the coated Nd-Fe-B samples show square-like hysteresis loops typical of performant hard magnet with a decreasing coercive field from 4 to 12 months (Fig. 3A). This decrease is related to the formation of soft magnetic phases. The loops feature also a progressive indentation at low field applied, with a progressive evolution from a pot-bellied to a wasp-waisted loop. From the data shown in Table 1, the reacted samples show a significant decrease in remanent specific magnetization (from 145 to 65.8 A^*m^2/kg) and a very low variation in saturation magnetization. However, this decrease does not appear to be time-related, considering that the sample reacted for 8 months has higher values than the other two, but related to a different amount of Nd-Fe-B hydrides (Table 2). This is related to different amounts of neo-formed, corrosion-related soft-magnetic phases. Contrarily, coercive field shows a progressive decrease from 1.2 T to 0.6 T.

The transition from a square-like ferromagnetic loop to the pot-bellied loop (after 4 and 8 months, as visible in the second quadrant of the hysteresis loops in Fig. 3A) remarks the presence of two magnetic phases, a soft magnetic phase (possibly NdFeB hydride whose magnetization reversal occurs at low magnetic field) and a hard

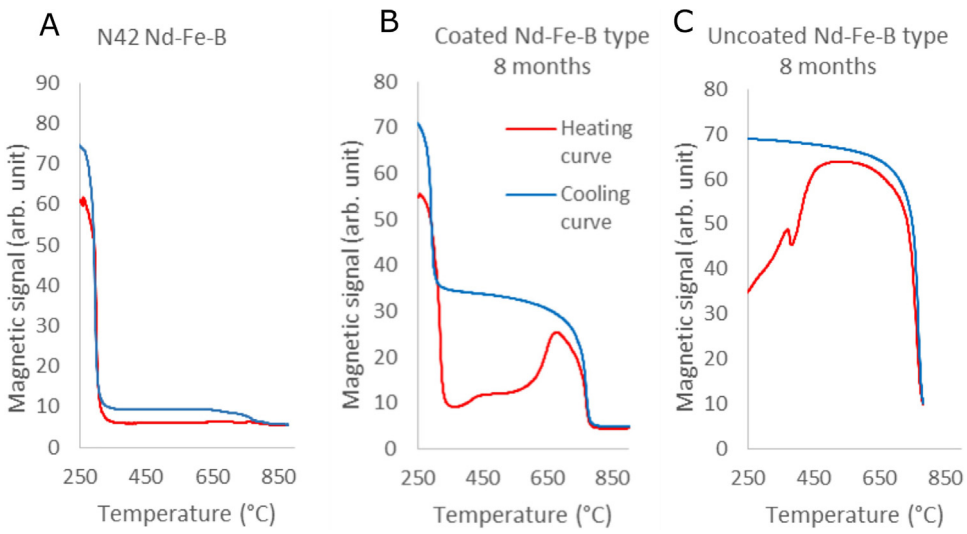

Fig. 4. Thermomagnetic curves of the coated (B) and uncoated (C) Nd-Fe-B samples reacted for 8 months compared with the starting N42 Nd-Fe-B material (A).

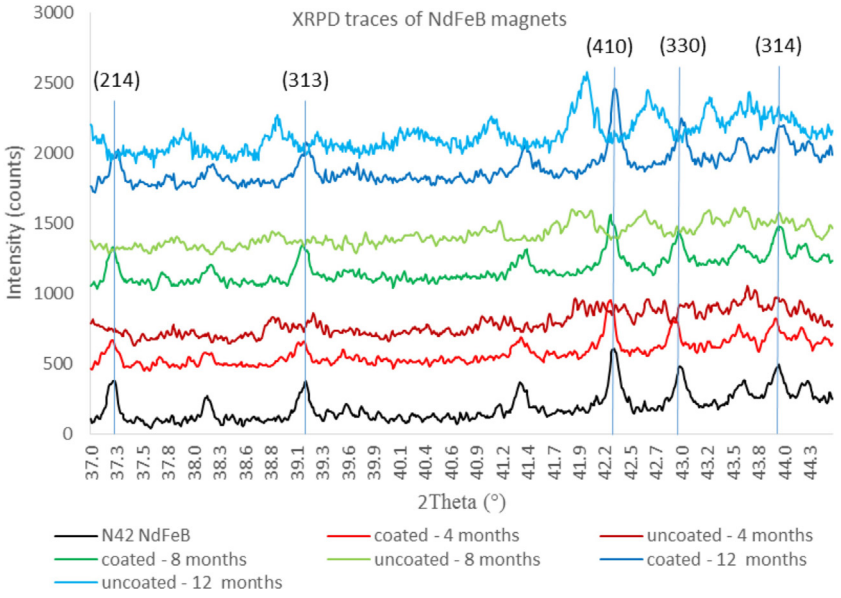

Fig. 5. XRPD traces of raw and corroded coated and uncoated Nd-Fe-B magnets. Peak labelling after [45]. Experiments performed using copper wavelength (0.15418 nm).

one ($Nd_2Fe_{14}B$) with larger coercive field. The transition to a wasp-waist loop after 12 months is indicative of superposition of two hysteresis loops of ferromagnetic materials with different coercive fields [35] (the initial hard φ-phase and a corrosion-related softer ferromagnetic Nd-Fe-B hydride).

Magnetization measurements on the uncoated Nd-Fe-B samples produced results coherent with the results shown in a previous research [6]. The uncoated samples feature a sharp transition from a high-coercive fields square-type loop of the raw N42 Nd-Fe-B to the loops typical of soft magnetic materials (Fig. 3B) of the samples reacted for more than 4 months, with zero coercive field and remanent specific magnetization. The sample reacted for four months features a wasp-bellied loop, with very low coercive field and remanent specific magnetization; the frequent indentations of the loop, suggest that this sample might have a complex mineralogy of the ferromagnetic component, with more than one phase, typically two coupled ferromagnetic phases with different coercive fields, and the soft magnetic phase as main component. In the uncoated samples, however, the contribution from mixed grain sizes [36] may play a considerable role together with the mineralogy. The samples subjected to a longer exposure (8 and 12 months) feature hysteresis loops typical of soft magnetic materials, with a vanished coercive field.

The trend of the saturation magnetization (Table 1) from the sample reacted for four months may indicate that the amount of the neo-formed soft magnetic phases increased with time.

The results of the thermomagnetic analysis (Table 1) on the coated Nd-Fe-B show a progressive increase of the Curie temperature from 310 °C to 350 °C. The samples reacted for 4 and 8 months feature two Curie points, one at 310 °C and one at 330 °C (Fig. 3), to testify the presence of another magnetic phase, likely a Nd-Fe-B hydride [37]. Among the uncoated Nd-Fe-B samples only one could be analysed and gave a temperature of 380 °C (Fig. 3), consistent with an $Nd_2Fe_{14}BH_{2-3}$ phase [37] or a complex mixture of Nd-Fe-B hydrides.

The uncoated Nd-Fe-B sample reacted for four months was affected by the explosion of the sealed silica ampoule upon heating at high temperature during the thermomagnetic measurement; this explosion most probably reflects the release of hydrogen from the Nd-Fe-B phase inducing large increase of the gas pressure.

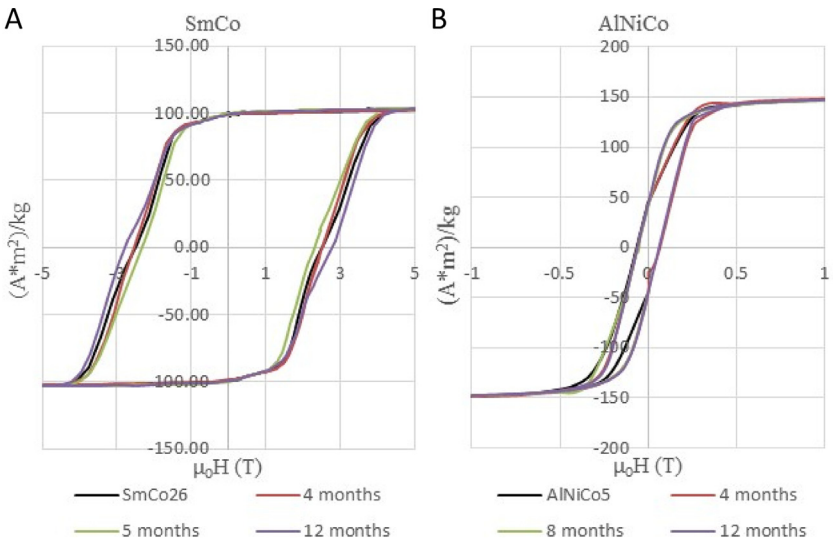

Fig. 6. Hysteresis loops of the raw and reacted SmCo magnets (A) and AlNiCo magnets (B).

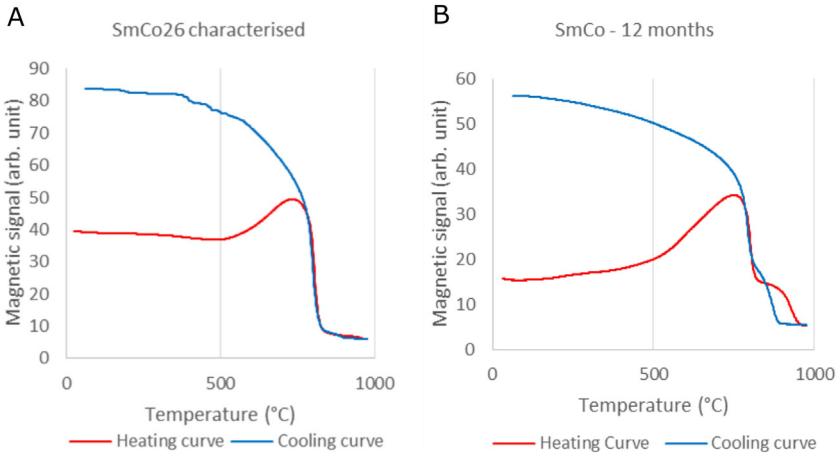

Fig. 7. Thermomagnetic curves of the characterised unreacted SmCo26 (A) and the SmCo sample reacted for 12 months (B).

The comparison between the thermomagnetic curves (Fig. 4) allows to differentiate the response of the materials from the raw material; the coated magnet (Fig. 4B) features two Curie points and increasing magnetization during heating with consequent Curie point at 790 °C. This is caused by formation of α-Fe upon irreversible transformation of the Nd-Fe-B hydride, which is decomposed in Nd-rich phases and α-Fe. The uncoated Nd-Fe-B sample (Fig. 3C) features complete irreversibility of the thermomagnetic curve, which testifies the metastability of the corroded material upon heating. The observed drop of the magnetic signal at 790 °C coincides with the Curie transition of the α-Fe.

X Ray Powder Diffraction analysis confirm that the corrosion process affected both the coated and uncoated magnets. A significant shift of the diffraction peaks to lower 2θ angles is registered for the uncoated magnets (Fig. 5), consistent with an increasing volume of the unit cell by hydrogen insertion within the interstitial sites of the main phase (φ-phase); the traces of the coated magnets feature a smaller shift but also exhibit the presence of reduced peak intensity and peak symmetry (Fig. 4).

XRPD semi-quantitative analysis on the run samples show that uncoated Nd-Fe-B magnets develop great quantities of hydrides, which become predominant in the samples. The coated Nd-Fe-B samples feature dominant unreacted φ-phase and variable amounts of hydrides, with a maximum in the 12 months reacted sample.

4.2. SmCo magnets

Magnetization analysis on the corroded SmCo magnets returned hysteresis loops closely resembling the starting material (Fig. 6A). Remanent specific magnetization and Saturation magnetization values (Table 3) are constant at 99 and 102.3 A*m^2/kg respectively. The coercive field values H_c show slight deviations from the raw starting sample (H_c = 2.5 T) for the sample reacted for 5 months (H_c = 2.45 T) and for the sample reacted for 12 months (H_c = 2.85 T with a clear indentation at 2.3 T).

The thermomagnetic curve of the 12-months reacted sample (Fig. 7B) shows the presence of two Curie points, one at 825 °C, corresponding to the main SmCo magnetic phase (as in the unreacted sample in Fig. 7A), and one at 960 °C. Larger Curie temperature is indicative of a larger Co content in the compound. The sample reacted for 5 months shows a secondary Curie temperature at 930 °C (Table 3). The secondary phase is likely metastable upon heating, and transforms to a more stable phase with a Curie temperature at 900 °C (cooling curve in Fig. 7B). The intrinsic magnetic parameters (remanent specific and saturation magnetization) are not sensitive, but the extrinsic parameter (coercive field) appears to be related to this secondary phase.

Based on the data available, the identification of these secondary, corrosion-related phase resulted a non-trivial case. A similar magnetic behaviour was observed by Isnard et al. [38] and

Table 3
List of hysteretic properties and Curie temperatures of the SmCo samples. In brackets the Curie temperatures of the accessory corrosion-related magnetic phases are presented.

	Duration (months)	Weight (gr)	Coercive field (T)	Remanent specific magn. (A^*m^2)/kg	Specific saturation magn. (A^*m^2)/kg	T_C (°C)
Raw		0.2937	2.5	99	102.3	825
Reacted	4	0.4170	2.5	99	102.3	825 (960)
	5	0.3563	2.45	99	102.3	825 (930)
	12	0.3521	2.85	99	102.3	825 (960)

Table 4
List of hysteretic properties and Curie temperatures of the AlNiCo samples.

	Duration (months)	Weight (gr)	Coercive field (T)	Remanent specific magn. (A^*m^2)/kg	Specific saturation magn. (A^*m^2)/kg	T_C (°C)
Raw		0.7320	0.065	44.8	163	860
Reacted	4	0.7352	0.065	40.8	153.76	860
	8	0.7425	0.065	42.7	159.86	860
	12	0.7433	0.065	43.7	157.54	860

an increase of T_C upon insertion of H, N or C in R_2M_{17} (R = Rare Earth Element, M = transition metal) was observed by Kianvash & Harris [39], Isnard et. al [40,41], Gubbens et al. [42] Kou et al. [43] Sun et al. [44]. Hence, the authors regard this corrosion-related ferromagnetic phase as being consistent with the presence of a hydrogen-decrepitated $Sm_2(Fe,Co)_{17}$-type phase together with the starting $Sm_2(Fe, Co)_{17}$ magnetic phase.

4.3. AlNiCo magnets

Magnetization analysis on the AlNiCo magnets do not show any relevant change in the hysteresis loops (Fig. 6B). The values of remanent specific magnetization do not deviate significantly from the initial raw material, and same applies for saturation magnetization; no changes occur to the thermomagnetic curves (Table 4).

5. Discussion

Following the previous paper by Harley et al. [6], the magnetization and thermomagnetic analysis on the three reacted permanent magnets and the comparison with the properties of the starting materials allowed to classify the magnets on their reactivity and identify potential candidates for short- and long-term monitoring of the EBS under the conditions explored in this paper:

- Weakly reactive magnet: the grade AlNiCo5 permanent magnet, even after 12 months continuous reaction featured only small deviations of remanent specific and saturation specific magnetization from the starting material. No changes in coercive field or thermomagnetic behaviour occurred.
- Moderately reactive magnet: the SmCo magnets did not show significant variations of the hysteretic parameters, but the thermomagnetic analyses uncovered an ongoing reaction leading to the formation of a secondary corrosion-related phase, that the authors believe being a hydrogen-decrepitated ferromagnetic high-coercive field Sm_2M_{17}-type phase.
- Highly reactive magnet: the grade N42 Nd-Fe-B magnets offered exceptional results either for the non-coated or coated samples. All the samples featured clear variation of the hysteretic properties after only four months, with the uncoated Nd-Fe-B showing a transition from hard magnetic to soft magnetic behaviour and the coated Nd-Fe-B a progressive time-dependent decrease in the coercive field and remanent specific magnetization. XRPD analysis showed that the corroded main magnetic phase was characterised by a shift of diffraction peaks towards lower diffraction angles, indicative of an increasing cell volume, probably due to hydrogen absorption. The corrosion process led to the formation of neo-formed softer magnetic materials (as shown by the trend of saturation magnetization) but was not possible to identify these phases through magnetic or XRPD analysis because these phases are likely nanoparticulates and/or amorphous.

6. Conclusions

Under the conditions tested in this work, Nd-Fe-B permanent magnets are steadily corroded by alkaline solutions in bentonite matrix, so they may offer a reliable real-time monitoring of water saturation of the EBS. SmCo magnets showed lower corrosion effects but formation of corrosion-related phases was found, to indicate that, under these conditions, their corrosion kinetics are significantly lower than Nd-Fe-B, but they could be useful for longer-term monitoring or ingression of highly aggressive solutions (eg. More saline solutions or brines).

Under the condition and the timescales here explored, AlNiCo magnets did not show appreciable changes in their hysteretic properties, although they, as like as SmCo, could be used for long-term monitoring of ingress of more aggressive solutions.

These results here represent a further refinement of the work undertaken by Harley *et al.* [6] and confirm that the magnetic monitoring is a reliable and safe alternative to the traditional monitoring methodologies.

Author contributions

S.H. conceived the project and general experimental design; N.R. and I.B. designed the experiments in detail; N.R performed the experiments; N.R. and O.I. carried out all the materials characterization and data analysis; N.R. wrote the paper.

Conflicts of interest

The authors declare no conflict of interest. The founding sponsors had no role in the design of the study; in the collection, analyses, or interpretation of data; in the writing of the manuscript, and in the decision to publish the results.

Acknowledgments

This research has been supported by ESPRC consortium grant EP/I036427/1 'SAFE Barriers – a Systems Approach For Engineered Barriers' (2012–2016). The present study was undertaken with funding from Radioactive Waste Management Limited (RWM)

(http://www.nda.gov.uk/rwm), a wholly-owned subsidiary of the Nuclear Decommissioning Authority.

References

[1] IAEA, Monitoring of Geological Repositories for High Level Radioactive Waste, 2001.
[2] European Commission, Thematic Network on the Role of Monitoring in a Phased Approach to Geological Disposal of Radioactive Waste, 2004, pp. 125.
[3] IAEA, IAEA Safety Standards: Geological Disposal of Radioactive Waste [Specific Safety Requirements No. WS-R-4], 2, 2006.
[4] D.G. Bennett, The Joint EC/NEA Engineered Barrier System Project: Synthesis Report (EBSSYN), 2010.
[5] IAEA, Monitoring and Surveillance of Radioactive Waste Disposal Facilities, 2014 http://www-pub.iaea.org/MTCD/Publications/PDF/Pub1640_web.pdf.
[6] S. Harley, N. Rigonat, I. Butler, Magnetic materials novel monitors of long-Term evolution of engineered barrier systems, Geosciences 6 (2016) 54, http://dx.doi.org/10.3390/geosciences6040054.
[7] Y. Li, H.E. Evans, I.R. Harris, I.P. Jones, The oxidation of NdFeB magnets, Oxid. Met. 59 (2003) 167–182, http://dx.doi.org/10.1023/A:1023078218047.
[8] J.J. Li, A.H. Li, M.G. Zhu, W. Pan, W. Li, Study on corrosion behaviors of sintered Nd-Fe-B magnets in different environmental conditions, J. Appl. Phys. 109 (2011) 3–6, http://dx.doi.org/10.1063/1.3565196.
[9] G. Yan, P.J. McGuiness, J.P.G. Farr, I.R. Harris, Environmental degradation of NdFeB magnets, J. Alloys Compd. 478 (2009) 188–192, http://dx.doi.org/10.1016/j.jallcom.2008.11.153.
[10] D.F. Cygan, M.J. McNallan, Corrosion of NdFeB permanent magnets in humid environments at temperatures up to 150 °C, J. Magn. Magn. Mater. 139 (1995) 131–138, http://dx.doi.org/10.1016/0304-8853(95)90037-3.
[11] J. Zheng, L. Jiang, Q. Chen, Electrochemical corrosion behavior of Nd-Fe-B sintered magnets in different acid solutions, J. Rare Earths. 24 (2006) 218–222, http://dx.doi.org/10.1016/S1002-0721(06)60097-5.
[12] J. Holc, S. Beseničar, D. Kolar, A study of Nd2Fe14B and a neodymium-rich phase in sintered NdFeB magnets, J. Mater. Sci. 25 (1990) 215–219, http://dx.doi.org/10.1007/BF00544210.
[13] R. Ramesh, J.K. Chen, G. Thomas, On the grain-boundary phase in iron rare-earth boron magnets, J. Appl. Phys. 61 (1987) 2993–2998, http://dx.doi.org/10.1063/1.337849.
[14] V. Yartys, O. Gutfleisch, I. Harris, Further studies of hydrogenation, disproportionation, desorption and recombination processes in a Nd5Fe2B6 boride, J. Alloys Compd. 253–254 (1997) 134–139, http://dx.doi.org/10.1016/S0925-8388(96)02996-9.
[15] S. Tencé, A. Wattiaux, M. Duttine, R. Decourt, O. Isnard, Magnetization measurements, specific heat, neutron diffraction and Mössbauer spectroscopy, J. Alloys Compd. 693 (2017) 887–894.
[16] B. Rupp, A. Resnik, D. Shaltiel, P. Rogl, Phase relations and hydrogen absorption of neodymium-iron-(boron) alloys, J. Mater. Sci. 23 (1988) 2133–2141, http://dx.doi.org/10.1007/BF01115780.
[17] V. Prakash, Z.H. Sun, J. Sietsma, Y. Yang, Electrochemical recovery of rare earth elements from magnet scraps- a theoretical analysis, ERES 2014 1 st, Eur. Rare Earth Resour. Conf. (2014) 163–170 http://www.eurare.eu/docs/eres2014/thirdSession/VenkatesanPrakash.pdf.
[18] L. Schultz, A. El-Aziz, G. Barkleit, K. Mummert, Corrosion behaviour of Nd-Fe-B permanent magnetic alloys, Mater. Sci. Eng. A. 267 (1999) 307–313, http://dx.doi.org/10.1016/s0921-5093(99)00107-0.
[19] K.E. Chang, G.W. Warren, The electrochemical hydrogenation of NdFeB sintered alloys, J. Appl. Phys. 76 (1994) 6262–6264, http://dx.doi.org/10.1063/1.358299.
[20] a. S. Kim, F.E. Camp, T. Lizzi, Hydrogen induced corrosion mechanism in NdFeB magnets, J. Appl. Phys. 79 (1996) 4840, http://dx.doi.org/10.1063/1.361626.
[21] H. Yang, S. Mao, Z. Song, The effect of absorbed hydrogen on the corrosion behavior of sintered NdFeB magnet, Mater. Corros. 63 (2012) 292–296, http://dx.doi.org/10.1002/maco.201005956.
[22] M. Sugimoto, K. Sohma, T. Minowa, T. Honshima, No Title, in: Jpn. Met. Soc. Fall Meet., 1987: p. 604.
[23] P.J. McGuiness, L. Fitzpatrick, V.A. Yartys, I.R. Harris, Anisotropic hydrogen decrepitation and corrosion behaviour in NdFeB magnets, J. Alloys Compd. 206 (1994) L7–L10, http://dx.doi.org/10.1016/0925-8388(94)90023-X.
[24] A. Ray, K. Strnat, Easy directions of magnetization in ternary R2(Co, Fe)17phases, IEEE Trans. Magn. 8 (1972) 516–518, http://dx.doi.org/10.1109/TMAG.1972.1067471.
[25] W.M. Pragnell, A.J. Williams, H.E. Evans, The oxidation morphology of SmCo alloys, J. Alloys Compd. 487 (2009) 69–75, http://dx.doi.org/10.1016/j.jallcom.2009.07.115.
[26] J.F. Liu, Y. Zhang, D. Dimitrov, G.C. Hadjipanayis, Microstructure and high temperature magnetic properties of Sm(Co, Cu, Fe, Zr)[sub z] (z = 6. 7–9.1) permanent magnets, J. Appl. Phys. 85 (1999) 2800, http://dx.doi.org/10.1063/1.369597.
[27] M.S. Walmer, C.H. Chen, M.H. Walmer, A new class of Sm-TM magnets for operating temperatures up to 550 °C, IEEE Trans. Magn. 36 (2000) 3376–3381, http://dx.doi.org/10.1109/20.908807.
[28] R. Gopalan, K. Muraleedharan, T.S.R.K. Sastry, A.K. Singh, Studies on structural transformation and magnetic properties in Sm 2 Co 17 type alloys, J. Mater. Sci. 6 (2001) 4117–4123.
[29] W.M. Pragnell, H.E. Evans, A.J. Williams, The oxidation kinetics of SmCo alloys, J. Alloys Compd. 473 (2009) 389–393, http://dx.doi.org/10.1016/j.jallcom.2008.05.083.
[30] M. McCaig, A.G. Clegg, Permanent Magnets in Theory and Practice, 2nd ed., Wiley, New York, 1987.
[31] C.A. Rochelle, G. Purser, A.E. Milodowski, D. Wagner, Results of Laboratory Carbonation Experiments on Nirex Reference Vault Backfill Cement, 2014.
[32] R. Fernández, J. Cuevas, L. Sánchez, R.V. de la Villa, S. Leguey, Reactivity of the cement-bentonite interface with alkaline solutions using transport cells, Appl. Geochem. 21 (2006) 977–992, http://dx.doi.org/10.1016/j.apgeochem.2006.02.016.
[33] R. Fernández, U. Mäder, M. Rodríguez, R. Virgil de la Villa, J. Cuevas, Alteration of compacted bentonite by diffusion of highly alkaline solutions, Eur. J. Mineral. 21 (2009) 725–735, http://dx.doi.org/10.1127/0935-1221/2009/0021-1947.
[34] A. Barlet, J.C. Genna, P. Lethuillier, Insert for regulating temperatures between 2 and 1000 K in a liquid helium dewar: description and cryogenic analysis, Cryogenics (Guildf) 31 (1991) 801–805, http://dx.doi.org/10.1016/0011-2275(91)90138-M.
[35] G.R. Kahler, L.H. Bennett, E. Della Torre, Coercivity and the critical switching field, Phys. B Condens. Matter. 372 (2006) 1–4, http://dx.doi.org/10.1016/j.physb.2005.10.005.
[36] A.P. Roberts, Y. Cui, K.L. Verosub, Wasp-waisted hysteresis loops: mineral magnetic characteristic and discrimination of components in mixed magnetic systems, J. Geophys. Res. 100 (17) (1995) (909–17,924).
[37] O. Isnard, W.B. Yelon, S. Miraglia, D. Fruchart, Neutron-diffraction study of the insertion scheme of hydrogen in Nd 2Fe14B, J. Appl. Phys. 78 (1995) 1892–1898, http://dx.doi.org/10.1063/1.360720.
[38] O. Isnard, S. Miraglia, D. Fruchart, D. Boursier, P. L'Héritier, Coercivity in hydrogen-decrepitated Sm2Co17-type compounds, J. Alloys Compd. 178 (1992) 23–28, http://dx.doi.org/10.1016/0925-8388(92)90243-3.
[39] A. Kianvash, I.R. Harris, Hydrogen decrepitation as a method of powder preparation of a 2:17-type, Sm(Co, Cu, Fe, Zr)8.92 magnetic alloy, J. Mater. Sci. 20 (1985) 682–688, http://dx.doi.org/10.1007/BF01026543.
[40] O. Isnard, S. Miraglia, J.L. Soubeyroux, D. Fruchart, P. l'Héritier, A structural analysis and some magnetic properties of the R2Fe17Hx series, J. Magn. Magn. Mater. 137 (1994) 151–156, http://dx.doi.org/10.1016/0304-8853(94)90201-1.
[41] O. Isnard, S. Miraglia, M. Guillot, D. Fruchart, High field magnetization measurements of sm $_2$ fe $_{17}$, sm $_2$ fe $_{17}$ n $_3$, Sm $_2$ fe $_{17}$ d $_5$, and pr $_2$ fe $_{17}$, Pr $_2$ Fe $_{17}$ N, J. Appl. Phys. 75 (1994) 5988–5993, http://dx.doi.org/10.1063/1.355485.
[42] P.C.M. Gubbens, A.M. van der Kraan, T.H. Jacobs, K.H.J. Buschow, Magnetic properties of the ternary carbides Tm2Fe17Cx, J. Magn. Magn. Mater. 80 (1989) 265–270, http://dx.doi.org/10.1016/0304-8853(89)90127-3.
[43] X.C. Kou, R. Grössinger, T.H. Jacobs, K.H.J. Buschow, Magnetocrystalline anisotropy and magnetic phase transition in R2Fe17Cx-based alloys, J. Magn. Magn. Mater. 88 (1990) 1–6, http://dx.doi.org/10.1016/S0304-8853(97)90003-2.
[44] H. Sun, J.M.D. Coey, Y. Otani, D.P.F. Hurley, Magnetic properties of a new series of rare-earth iron nitrides: r 2 Fe 17 N y (y approximately 2.6), J. Phys. Condens. Matter. 2 (1990) 6465–6470, http://dx.doi.org/10.1088/0953-8984/2/30/013.
[45] M. Sagawa, K. Hiraga, H. Yamamoto, Y. Matsuura, Permanent magnet materials based on the rare earth-iron-boron tetragonal compounds (invited), IEEE Trans. Magn. 20 (1984) 1584–1589, http://dx.doi.org/10.1109/TMAG.1984.1063214.